Hydrol. Earth Syst. Sci. Discuss., https://doi.org/10.5194/hess-2018-223
Manuscript under review for journal Hydrol. Earth Syst. Sci.
Discussion started: 2 May 2018

Hydrology and Earth System Sciences
Open Access
Discussions

The climate of desiccation in the SW Cape

Mark R. Jury

University of Zululand, KwaDlangezwa, South Africa

and Physics Dept, University of Puerto Rico Mayagüez, USA

Abstract

Hydro-meteorology conditions in the Southwest Cape of South Africa are analyzed for historical trends in satellite and station measurements. Results show an increase of coastal upwelling, low-level subsidence and shorter winters. The shearing by offshore easterly winds causes a circulation over the SW Cape which entrains dry air from the south coast upwelling zone. Potential evaporation exceeds precipitation and streamflow discharge has declined particularly northwest of the Hottentots Holland mountains. Many of Cape Town's water reservoirs are drying up, and show steep increases in surface temperature (+.2C/yr) and browning of perimeter vegetation. The unfavorable wind shear is compounded by negative sensible heat flux and a capping inversion, so alongshore winds and mountain-top clouds divert seaward, desiccating the upper Berg River catchment.

Key words: SW Cape, hydro-climate deficit

mark.jury@upr.edu

Hydrol. Earth Syst. Sci. Discuss., https://doi.org/10.5194/hess-2018-223
Manuscript under review for journal Hydrol. Earth Syst. Sci.
Discussion started: 2 May 2018

Hydrology and Earth System Sciences
Open Access
Discussions

1. Introduction

The southwestern (SW) Cape of South Africa (34S, 19E) lies at the transition between the sub-tropical easterly and mid-latitude westerly wind regimes, and has a semi-arid, rainy-winter climate. The adjacent interior (Karoo) has sparse vegetation fronted by coastal mountains over 1000 m. Past research on climate change at country-scale has found a ~0.02°C/yr increase of temperature (Kruger and Shongwe 2004; Morishima and Akasaka 2010) consistent with global averages, and mixed trends in rainfall (Tadross et al 2005; MacKellar et al 2014). Yet, water resources within reach of Cape Town's 4 M people (west of 20E) have dwindled to unsustainable levels (13% of storage capacity = 217 M m^3 < www.dwa.gov.za/Hydrology/ > as of April 2018). Water supplies are so scarce that numerous engineering projects are underway (Muller 2017), in addition to rationing of 50 L/day/person. Here an analysis of meteorological factors underlying the water deficit is conducted to promote awareness and strategic planning. During this era, global greenhouse gases have risen 2 ppm/yr, national industrial emissions exceeded 600M T/yr (Bekker et al 2008; DEAT 2009), and continental agricultural emissions reached 1350M T/yr (Semazzi and Song 2001; Sinha et al 2003).

2. Data and Methods

The SW Cape of South Africa (SA) has a dense network of rainfall, streamflow and potential evaporation stations maintained by the Dept of Water Affairs (DWA). Here monthly long-term records with > 90% completeness are obtained in the Upper Berg River catchment, (lat/lon): -33.65/19.01; -33.83/19.08; -33.93/19.06; -34.32/18.99. High resolution NOAA MODIS satellite data are analyzed for land surface temperature and vegetation color. The dispersion of urban emissions is represented by OMI satellite NO_2 measurements (Bucsela et al 2013) averaged 2010-2017. Gridded fields are generated by data assimilation of in-situ and satellite observations, and include: CRU4 rainfall and Palmer Drought Severity Index (PDSI; Harris et al 2014); NCEP2 atmosphere reanalysis (Kanamitsu et al 2002); NOAAoi2 sea surface temperature (SST; Reynolds et al 2007), NOAA net outgoing long-wave radiation (OLR; Lee 2015), CHIRPS2 and GPCC7 rainfall (Funk et al. 2015;

Schneider et al 2014), MERRA2 atmosphere reanalysis (Reinecker et al 2011, Molod et al 2015), and SODA3 ocean reanalysis (Carton and Giese 2008).

Monthly averages over the key area: 34.5-33.5S, 18.5-19.5E are used to calculate trends by linear regression, as in (Jury 2013, 2018). The rate of change or slope is evaluated across the field (for maps and sections) and key area (for time series) over the period 1980-2017 using the above reanalysis datasets. Statistical evaluations use the Pearson's 2-tailed t-test and degrees of freedom. With a DF = 37, 90% confidence is achieved by $r > |0.27|$ or $r^2 > .06$. Some records are longer: the DWA stations 1956+, GPCC7 and CRU4 rainfall / PDSI 1901+; while some are shorter: MODIS satellite data 2000+. Ranking the satellite land surface temperature, a hot dry spell of 1-8 January 2011 is analyzed using reanalysis fields and SA Weather Service hourly observations and radiosonde profiles from Cape Town airport (CPT). The mesoscale structure of SW Cape hydrology is linked to the uptake of climate change from rising greenhouse gases, and natural multi-year fluctuations (Poccard et al 2000).

3. Results

3.1 SW Cape local and regional trends

The SW Cape urban NO_2 emissions (Fig 1a) illustrate the atmospheric impact of 4 M residents and their resource needs. Higher pollution concentrations at 33.75S, 18.75E extend northward in a broad arc, according to OMI satellite measurements averaged 2010-2017. Values > 10 µg /m^3 are consistent with in-situ data (SOER 2017). The wind and rainfall trend map (Fig 1b) illustrates a cyclonic circulation and drying to the northwest of the mountains.

SST trends (Fig 1c) are positive offshore but negative nearshore (cf. Rouault et al 2010), and point to intensification of coastal upwelling by the southeasterly winds 1980-2017. The offshore Ekman transport and cyclonic wind shear lifts cool water over the shelf, with desiccating effect as seen below.

Hydrol. Earth Syst. Sci. Discuss., https://doi.org/10.5194/hess-2018-223
Manuscript under review for journal Hydrol. Earth Syst. Sci.
Discussion started: 2 May 2018

Land surface temperatures (Fig 2c) display increases of 0.1 C/yr (Fig 2a) in the MODIS era (2000-2017). Values are highest at the Berg River dam near Franschoek (0.2 C/yr), ~10 times above global and national means (Kruger and Shongwe 2004). Such a high rate of warming is caused by receding water around the perimeter of the reservoir, and heating of bare soil during periods of high solar radiation (Appendix 1 photo; cf. Earth observatory 2018). In conjunction, the vegetation color fraction has declined around the Berg River dam near Franschoek (Fig 2d). A 'browner' surface is also found in the Theewaterskloof Reservoir (-.02 /yr) and west of the Hottentots Holland mountains. Yet greening is noted in the MODIS era (2000-2017) to the east of 19.1E (+.01 /yr), and Chirps2 rainfall trends are weakly positive there (Fig 2e) due to the up-slope of easterly winds.

The main hydrological concern is the diminishing rainfall northwest of the Hottentots Holland, across the populated Cape Flats. The annual rain trend is -.5 mm month^{-1}/yr in the vicinity of Wellington (33.64S, 19.00E). The histogram of NOAA infrared vegetation temperature, comparing the 1982-88 and 2010-16 era (Fig 2f), illustrates shifts in both cold and warm seasons. In the 12.5C range typical of winter, there was a reduction from 18 to 12 months. In the 30-32.5C range typical of summer, there was huge increase from 3 to 24 months. The histogram indicates a desiccating regime, which is placed in context below.

3.2 Temporal characteristics

In this section, a temporal analysis is presented for station observations in the key area. Ensemble rainfall trends per month (Fig 3a) are downward except for small rises in August and November. Months with significant declines include January, March, October and December. Months with the largest drying trends are May and September, at the beginning and end of winter. Streamflow discharge shows a downward trend in the Upper Berg River catchment (Fig 3b). Of note are the low summer flows in the early 1970s that culminated in three dry years: 1978-1980. Streamflow discharge recovered over a lengthy era from 1981 to 2014, but then declined in both winter and summer to almost zero by 2017 (end of record).

Hydrol. Earth Syst. Sci. Discuss., https://doi.org/10.5194/hess-2018-223
Manuscript under review for journal Hydrol. Earth Syst. Sci.
Discussion started: 2 May 2018

A longer term perspective is offered by CRU4 PDSI anomalies (Fig 3c) that show a persistent downward trend through the 20th century, consistent with Wolski (2018). The 1970s dry spell re-curred in the most recent decade (2010+). Apart from the 1950s and 1980s, the water budget has shown deficit conditions: potential evaporation exceeded precipitation. The downward trend in PDSI is 17% of total variance. The DWA pan evaporation measurements (Fig 3d) have a weak up-ward trend since 1956. There is a large annual cycle that peaks in summer each year, when desic-cating weather prevails.

Seasonal variability tends to obscure the climate change signal, so individual monthly trends are considered. The linear upward trend in potential evaporation accounts for 15% of variance from January to March with a summer-time slope of 0.15 mm day^{-1}/yr in the period 1956-2017. Similar-ly, the satellite net OLR shows positive trends in the key area (reduced cloud cover), as listed in Table 2. Desiccation is most significant in the December to April months (1979-2017).

3.4 Regional drivers of desiccation

Trends are mapped in vertical sections along 34S from 15.5E to 24.5E in Fig 4a-d. A surprizing result is that subsident trends within the easterlies are strongest south of the Langeberg mountains (20-24E). Air temperature trends are relatively weak at .01 C/yr in the 1000-900 hPa layer. Warming increases westward consistent with a change from moistening 21-24E to drying 16-19E. Turning attention to the shelf oceanography, it is evident that upwelling has intensified (-.02 C/yr) from surface to 40 m depth to the east of 19E, despite a warming trend elsewhere in the period 1980-2016. The warm air / cool sea trend causes sensible heat flux (Q_h) to decline -.2 W m^{-2}/yr. Hence the lower atmosphere is stabilized along the South Cape coast. As a secondary consequence, the subsidence inversion strengthens and caps the surface easterly flow, as outlined in Jury and Reason (1989). The Froude number, calculated from $F = U / NH$, offers a way to determine whether the airflow will ascend the SW Cape mountains ($F \geq 1$) or go around them ($F<1$). With a westerly wind of $U = 10$ m/s, a mountain height of $H = 10^3$ m, and a winter-time unstable lapse rate of N =

Hydrol. Earth Syst. Sci. Discuss., https://doi.org/10.5194/hess-2018-223
Manuscript under review for journal Hydrol. Earth Syst. Sci.
Discussion started: 2 May 2018

$((g / \theta_o)(d\theta / dz))^{0.5} \sim 10^{-2}$, the airflow lifts over the mountains causing stratiform rainfall. Under the summer-time easterly wind regime, the U and H values are the same. But surface cooling and low-level warming induce a stable lapse rate of N ~ 2 10^{-2}, so F = 0.5. The airflow is diverted around the mountains instead of going over the Hottentots Holland; leaving them sunny and prone to desiccation.

As the sub-tropical ridge shifts poleward, there is a broad zone of intensifying easterly flow from 32-40S, 0-40E (Fig 4e). Evidence of Venturi acceleration at the southern tip of Africa (35S, 20E) emerges in zonal wind trends of -.05 m s^{-1}/yr (1980-2017). The associated easterly shear spins-up a wind rotor over the SW Cape (cf. Fig 1b) with desiccating consequences.

The change of winds from easterly to southeasterly can be traced to three influences: firstly the change in coastal orientation, secondly the day-time thermal gradient / seabreeze, and thirdly the land-friction / Ekman spiral. Seabreeze forcing is: $dV = ((g\, H / \theta)\, d\theta / dy)\, dt$ with g gravity, H surface layer ~ 30 m, potential temperature θ ~ 300K, dθ ~ 3K sea-land increase, and dy, dt are length, time scales (~ 2 10^4). The Ekman spiral effect is: $V = U_g\, (e^{-az} \sin(-az))$, with U_g geostrophic easterly wind (~ 10 m/s), $a = (f / 2\, K)^{0.5}$, z = 30 m, coriolis f = 7 10^{-5} s^{-1}, and terrestrial eddy viscosity K > 2 m^2 s^{-1}. As the easterly winds turn equatorward, subsidence is generated: $W = V(\Delta Z)(\beta/f)$, with V ~ 5 m/s, thickness $\Delta Z \sim 5\ 10^3$ m, $\beta = df/dy \sim -1.5\ 10^{-11}$ s^{-1} m^{-1}, and f = 7 10^{-5} s^{-1}. Sinking motion of W ~ -5 10^{-3} m/s actively dries out the lower atmosphere. The pattern of -5 m/s zonal wind anomalies for Dec-Jan 2011 (Fig 4f) leads into a case study of desiccation.

3.3 Dry spell case study

Ranking the MODIS day-time land surface temperature record in the SW Cape (33.5-34.5S, 18.5-19.5E), the period 1-8 January 2011 is the hottest case (42 C) in the period 2000-2017. The map of surface temperatures (Fig 5a) reveals a narrow strip of cool conditions along the windward coastal promontories such as Cape Point (20 C). However across the Cape Flats and interior valleys (Berg, Brede) the day-time land surface temperatures exceed 50 C! The air-flow at 850 hPa (Fig 5b) shows

Hydrol. Earth Syst. Sci. Discuss., https://doi.org/10.5194/hess-2018-223
Manuscript under review for journal Hydrol. Earth Syst. Sci.
Discussion started: 2 May 2018

cyclonic curvature and > 5 m/s easterlies over the ocean to the south. The vegetation color fraction (Fig 5c) diminished 0.1 from the end of December to mid-January 2011 in the Upper Berg River catchment, west of Hottentots Holland mountains. A vertical section analysis shows a strong easterly 'jet' capped by an inversion (Fig 5d) in the period 1-8 January 2011. In the offshore zone (35S), the near-surface winds were 10 m/s and temperatures were < 20 C. During this dry spell, coastal upwelling caused SST < 15 C (Fig 5e). A consequence of warm air overlying cool sea is thermal stability, which inhibits the inland penetration of moisture (cf. Fig 5b). The CPT weather station reported desiccating weather conditions 3-6 January (Fig 5f) characterized by T_{max} = 34 C and T_{dew} = 16 C. Southerly winds strengthened 3-4 January to 35 km/hr and then abated following passage of the South Atlantic high pressure cell. CPT radiosonde profiles on 6 January 2011 (Appendix 2) describe characteristics in the 400-700 m subsidence inversion: 110º / 14 kt winds, 32.6 C temperature, -14.6 C dewpoint, and specific humidity 1.36 g/kg due to entrainment of dry air from aloft (cf. 500 hPa sinking motions in Fig 5e). Many DWA stations near Wellington recorded potential evaporation > 12 mm/day!

4. Summary

Hydro-meteorology conditions and trends in the Southwest Cape of South Africa have been studied using historical satellite and station measurements, and gridded reanalysis fields. Results show an increase of coastal upwelling, low-level subsidence and shorter winters. The sub-tropical ridge has shifted poleward causing an increase of easterly winds along 35S. The wind shear induces a cyclonic rotor over the SW Cape, which entrains dry air from the interior Karoo and south coast upwelling zone. Precipitation has declined particularly northwest of the Hottentots Holland mountains and many water reservoirs show steep increases in surface temperature (+.2 C/yr) and browning of perimeter vegetation since 2000. The unfavorable wind shear is compounded by negative sensible heat flux and a capping inversion, so winds and mountain-top clouds divert seaward. The regime shift from mid-latitude westerly winds and winter rainfall, to sub-tropical easterly winds and summer dry spells has depleted water resources. Hence recycling, desalination, importation, and aquifer

Hydrol. Earth Syst. Sci. Discuss., https://doi.org/10.5194/hess-2018-223
Manuscript under review for journal Hydrol. Earth Syst. Sci.
Discussion started: 2 May 2018

Hydrology and Earth System Sciences
Open Access
Discussions

extraction projects are underway (EWN 2018), and water conservation has become rooted in popular thinking and community awareness. The above results contribute to this educational initiative, and suggest that water deficits in the SW Cape are here to stay.

5. Acknowledgements

S.A. Dept of Education SAPSE funding support is acknowledged. Data were analyzed from websites: IRI Climate Library, KNMI Climate Explorer, APDRC Hawaii, SA Dept of Water Affairs, and Wundermap.

6. References

Bekker B, Eberhard A, Gaunt T, Marquard A (2008) South Africa's rapid electrification programme: Policy, institutional, planning, financing and technical innovations. Energy Policy, 36: 3125-3137

Bucsela EJ and co-authors (2013) A new stratospheric and tropospheric NO2 retrieval algorithm for nadir-viewing satellite instruments, applications to OMI, Atmos Meas Tech, 6: 2607-2626

Carton JA and Giese BS (2008) A reanalysis of ocean climate using Simple Ocean Data Assimilation (SODA). Mon Wea Rev, 136: 2999-3017

DEAT (2009) Greenhouse gas inventory of South Africa: 1990-2000. Pretoria. cited in: www.erc.uct.ac.za/Information/Climate%20change/Climate_change_info-complete.pdf

Earth Observatory (2018) Satellite photos accessed April 2018 via < earthobservatory.nasa.gov/IOTD/view.php?id=91649 >

EWN (2018) news website accessed April 2018 via < ewn.co.za/2018/01/10/ct-hopes-to-have-3-desalination-plants-running-by-march >

Funk CC and co-authors (2014) A quasi-global precipitation time series for drought monitoring: U.S. Geological Survey Data Series 832: 4 pp. < dx.doi.org/110.3133/ds832 >

Hydrol. Earth Syst. Sci. Discuss., https://doi.org/10.5194/hess-2018-223
Manuscript under review for journal Hydrol. Earth Syst. Sci.
Discussion started: 2 May 2018

Harris I, Jones PD, Osborn TJ, Lister DH (2014) Updated high-resolution grids of monthly climatic observations, the CRU[v4] Dataset. Int J Climatol, 34: 623-642

Jury MR and Reason CJ (1989) Extreme subsidence in the Agulhas-Benguela air mass transition, Bound Layer Meteorol, 46: 35-51

Jury MR (2013) Climate trends in southern Africa. S Afr J Science, 109: 53-63

Jury MR (2018) Climate trends across South Africa since 1980. Water SA: (in press).

Kanamitsu M et al (2002) NCEP–DOE AMIP-II Reanalysis (R-2). Bull Amer Meteor Soc, 83: 1631-1643

Kruger AC, Shongwe S (2004) Temperature trends in South Africa: 1960–2003. Int J Climatol, 24: 1929-1945

Lee H-T (2014) Climate algorithm theoretical basis document: Outgoing long-wave radiation (OLR). NOAA's Climate Data Record (CDR) Program, CDRP-ATBD-0526, 46 pp.

MacKellar N, New M, Jack C (2014) Observed and modelled trends in rainfall and temperature for South Africa: 1960–2010. S Afr J Sci, 110: 1-13

Mitchell TD, Jones PD (2005) An improved method of constructing a database of monthly climate observations and associated high-resolution grids, Intl J Climatol, 25: 693-712

Morishima W, Akasaka I (2010) Seasonal trends of rainfall and surface temperature over Southern Africa. African Study Monographs, 40: 67-76

Molod, A., L. Takacs, M. Suarez and J. Bacmeister. 2015. Development of the GEOS-5 atmospheric general circulation model: evolution from MERRA to MERRA2, Geosci Model Dev, 8: 1339-1356

Muller M (2017) Understanding Cape Town's Water Crisis. Civil Engineering, accessed via <

Hydrol. Earth Syst. Sci. Discuss., https://doi.org/10.5194/hess-2018-223
Manuscript under review for journal Hydrol. Earth Syst. Sci.
Discussion started: 2 May 2018

Hydrology and Earth System Sciences
Open Access
Discussions

ssrn.com/abstract=2995937 >

Poccard I, Janicot S, Camberlin P (2000) Comparison of rainfall structures between NCEP/NCAR reanalyses and observed data over tropical Africa. Climate Dynamics, 16: 897-915

Reynolds RW, Smith TM, Liu C, Chelton DB, Casey KS, Schlax MG (2007) Daily high-resolution blended analyses for sea surface temperature. J Climate, 20: 5473-5496

Rienecker MM and co-authors (2011) MERRA: NASA's Modern-Era Retrospective Analysis for Research and Applications. J Climate, 24: 3624-3648

Rouault M, Pohl B, Penven P (2010) Coastal oceanic climate change and variability from 1982 to 2009 around South Africa. Afr J Marine Science, 32: 237-246

Schneider U, Becker A, Finger P, Meyer-Christoffer A, Ziese M and Rudolf B (2014) GPCC's new land surface precipitation climatology based on quality-controlled in situ data and its role in quantifying the global water cycle. Theor Appl Climatol, 115: 15-40

Semazzi FHM, Song Y (2001) A GCM study of climate change induced by deforestation in Africa. Climate Res, 17: 169-182

Sinha P et al (2003) Emissions of trace gases and particles from savanna fires in southern Africa. J Geophys Res, 108: d13, 8487, doi10.1029/2002JD002325

SOER (2017) State of the Environment Report, Western Cape air quality, accessed April 2018 via: < W_Cape_SOER_08_Air_Quality.pdf >

Tadross M, Jack C, Hewitson B (2005) On RCM-based projections of change in southern African summer climate. Geophys Res Lett, 32: L23713, doi:10.1029/2005GL024460.

Wolski P (2018) How severe is Cape Town's 'Day Zero' drought? Significance, 15: 24-27

Table 1 Datasets used in the trend analysis. References are listed in text; web sources are given in acknowledgement.

	name	resolution
CHIRPS2	Climate hazards infrared precipitation with station v2 (Meteosat + gauge)	5 km
CRU4	Climate Research Unit v4 (gauge-based, PDSI, rainfall)	50 km
DWA	Dept of Water Affairs station data for streamflow and potential evaporation	1 km
GPCC7	Global Precipitation Climatology Center v7 (gauge-based)	50 km
MERRA2	Modern Era Reanalysis for Research and Applications v2 (model-based)	60 km
NCEP2	National Center for Environmental Prediction v2 Reanalysis	180 km
NOAA	National Oceanic and Atmospheric Administration (satellite data)	5-100 km
OMI	Ozone Monitoring Instrument (AURA satellite) v3	25 km
SODA	Simple Ocean Data Assimilation v3 (model-based ocean reanalysis)	50 km

Hydrol. Earth Syst. Sci. Discuss., https://doi.org/10.5194/hess-2018-223
Manuscript under review for journal Hydrol. Earth Syst. Sci.
Discussion started: 2 May 2018

Hydrology and Earth System Sciences
Open Access
Discussions

Table 2 Trends in satellite net OLR averaged over the key area, expressed as the correlation between the linear slope and the time series, per month in the period 1979-2017. Insignificant p-values are confined to May-June. Positive r-values refer to reduced cloud cover and desiccation.

months	r-value	p-value
Jan	0.646	0.000
Feb	0.406	0.009
Mar	0.381	0.015
Apr	0.573	0.000
May	0.214	0.192
Jun	0.206	0.208
Jul	0.441	0.005
Aug	0.396	0.013
Sep	0.461	0.003
Oct	0.408	0.010
Nov	0.322	0.045
Dec	0.508	0.001

Hydrol. Earth Syst. Sci. Discuss., https://doi.org/10.5194/hess-2018-223
Manuscript under review for journal Hydrol. Earth Syst. Sci.
Discussion started: 2 May 2018

Figures

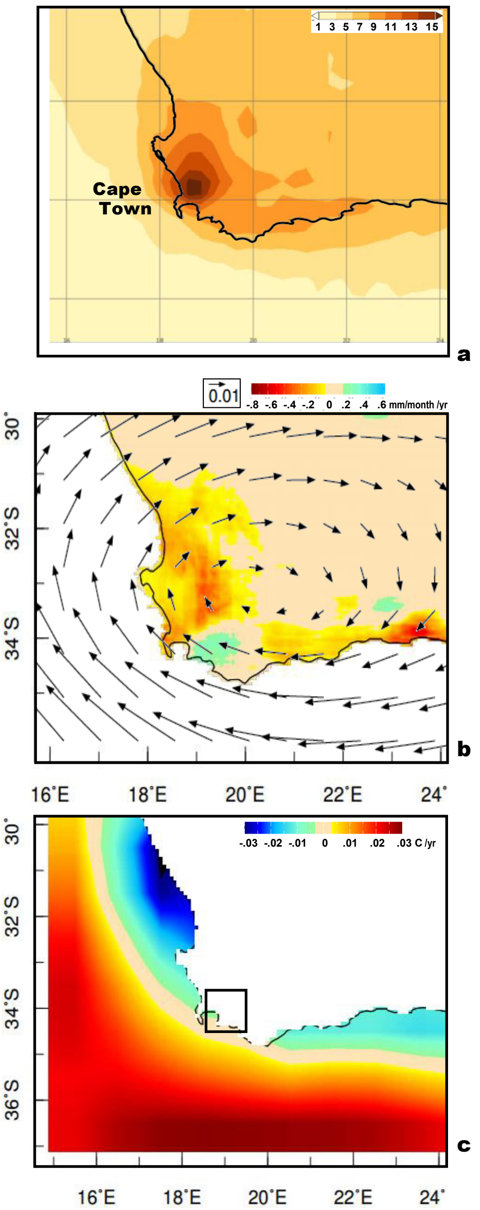

Figure 1 (a) 2010-2017 average OMI satellite NO2 concentration illustrating urban emissions (µg/m^3). The 1981-2017 linear trend of: (b) 1000-925 hPa NCEP2 wind vectors (m/s /yr) and Chirps 2 rainfall (shading), (c) NOAA oiv2 SST. Map covers the SW Cape region; square in (c) is the key area for temporal analysis.

Hydrol. Earth Syst. Sci. Discuss., https://doi.org/10.5194/hess-2018-223
Manuscript under review for journal Hydrol. Earth Syst. Sci.
Discussion started: 2 May 2018

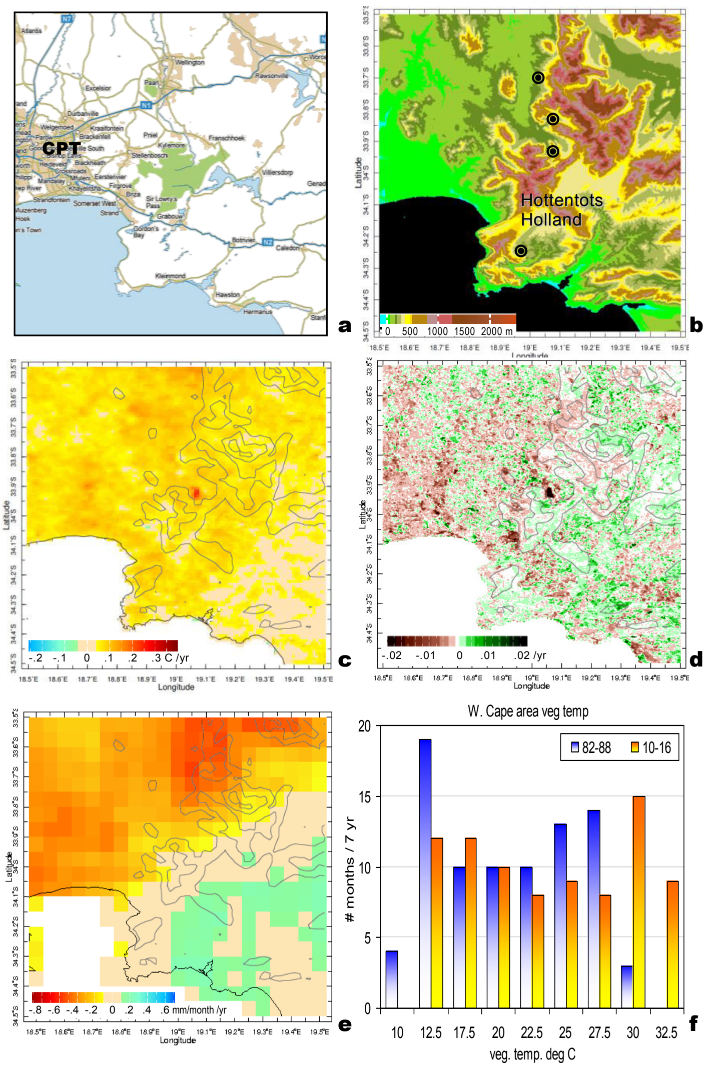

Figure 2 SW Cape (a) locations, (b) topography and DWA stations, (c) Modis surface temperature trend (2000-2017), (d) vegetation fraction trend (2000-2017), (e) Chirps2 rainfall trend (1981-2017), (f) histogram of NOAA satellite vegetation temperature: # months per bin (C) in the first versus last 7 yr.

Hydrol. Earth Syst. Sci. Discuss., https://doi.org/10.5194/hess-2018-223
Manuscript under review for journal Hydrol. Earth Syst. Sci.
Discussion started: 2 May 2018

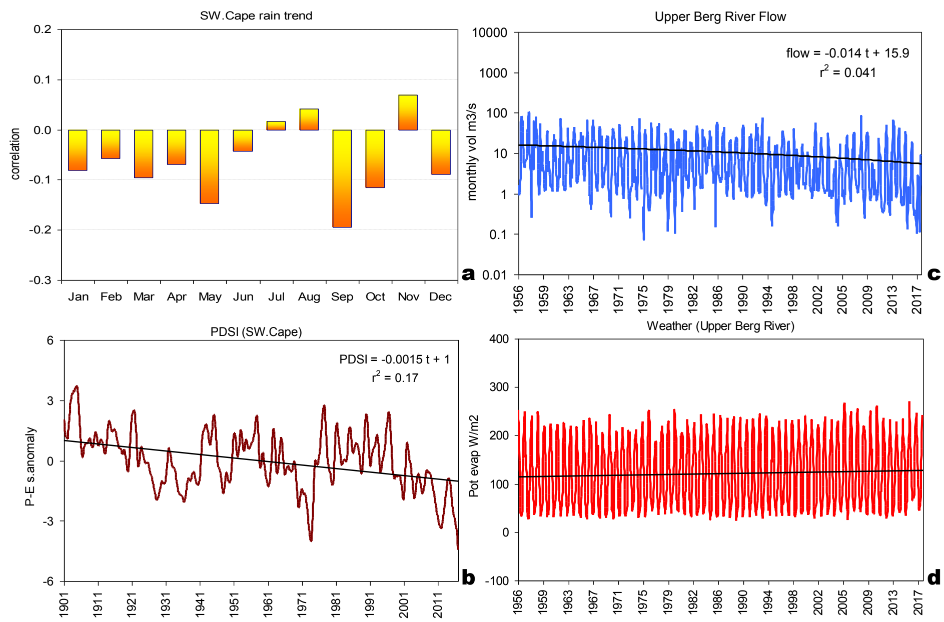

Figure 3 (a) Bar-chart of temporal correlation of SW Cape rainfall with linear trend, per month, average of three datasets (1901+). (b) Time series of CRU4 PDSI representing precipitation minus potential evaporation anomalies (1901+). Time series of averaged station data in the upper Berg River catchment: (c) streamflows (log-scale) and (d) potential evaporation (1956+). Trends are given and variance is listed for PDSI anomalies.

Hydrol. Earth Syst. Sci. Discuss., https://doi.org/10.5194/hess-2018-223
Manuscript under review for journal Hydrol. Earth Syst. Sci.
Discussion started: 2 May 2018

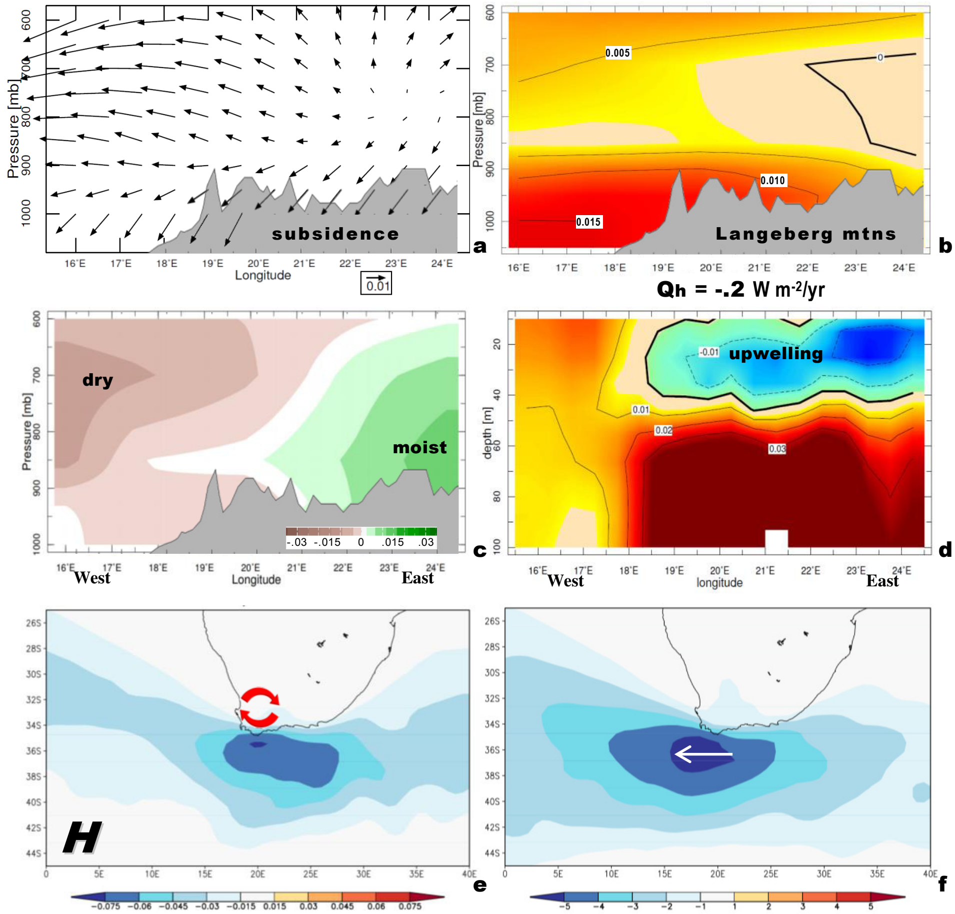

Figure 4 Trend in vertical section west-east averaged in SW Cape latitudes (33.5-35S) of (a) zonal circulation (vectors U,W), (b) air temperature (C/yr), (c) specific humidity (ppt/yr), and (d) sea temperature (C/yr); extending from 15.75E to 24.5E (1980+). (e) Dec-Jan trend of surface zonal wind (1979+) m/s /yr and (f) surface zonal wind anomaly Dec-Jan 2011 m/s. Qh (between b,d) = trend of sensible heat flux. The SW Cape rotor is depicted in (e).

Hydrol. Earth Syst. Sci. Discuss., https://doi.org/10.5194/hess-2018-223
Manuscript under review for journal Hydrol. Earth Syst. Sci.
Discussion started: 2 May 2018

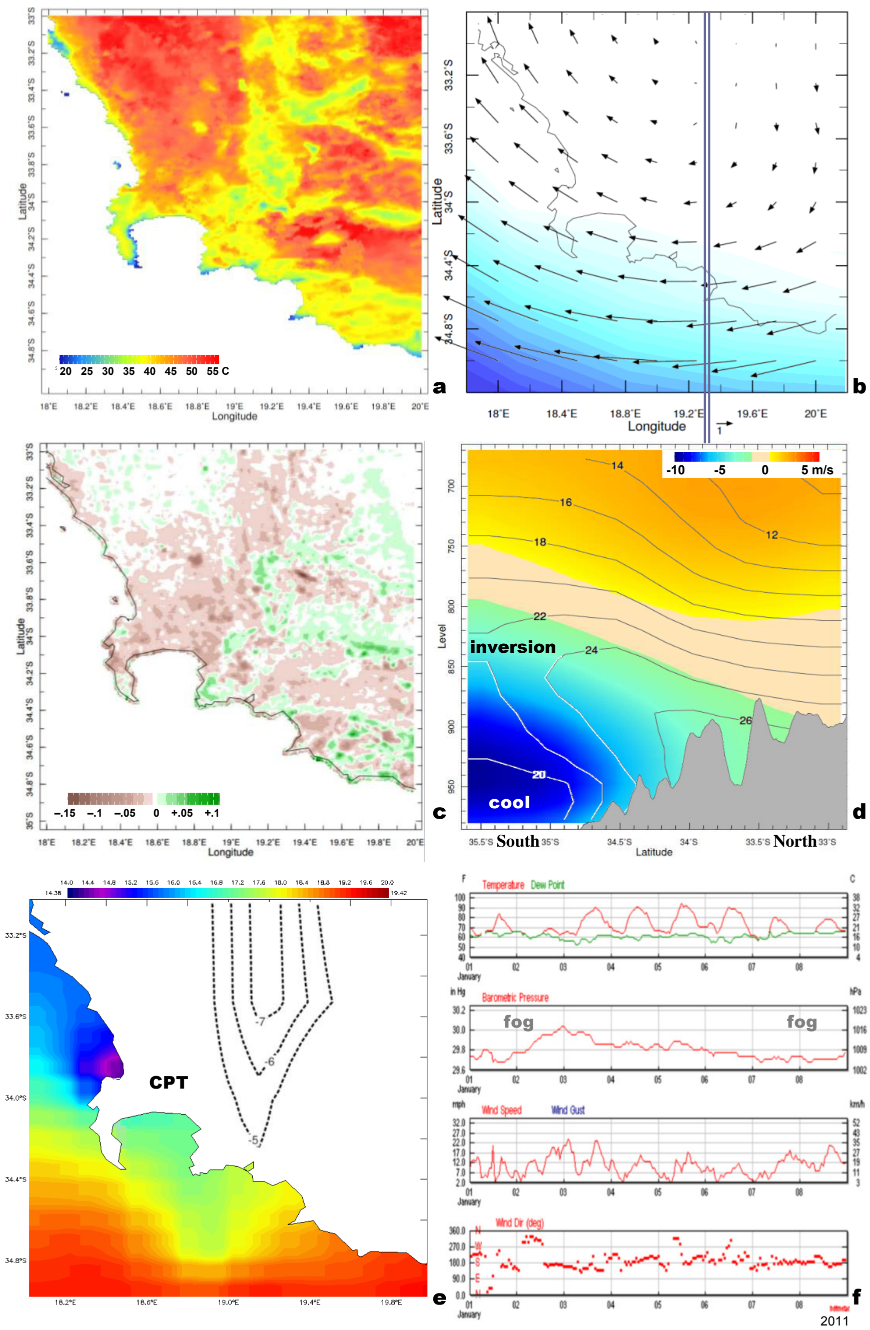

Figure 5 Case study of hot dry weather 1-8 Jan 2011, (a) day-time land surface temperature, (b) 850 hPa wind vectors and latent heat flux (blue shading 5-50 W m^{-2}), (c) change in vegetation fraction before to after, (d) vertical section on 19.33E (line in (b) of zonal wind (shaded) and temperature (contour) with mountain profile, (e) sea surface temperature and 500 hPa vertical motion (contours $x10^{-3}$ m/s), (f) hourly weather observations at CPT airport during the case study.

Hydrol. Earth Syst. Sci. Discuss., https://doi.org/10.5194/hess-2018-223
Manuscript under review for journal Hydrol. Earth Syst. Sci.
Discussion started: 2 May 2018

Hydrology and Earth System Sciences
Open Access
Discussions

Appendix 1

Aerial photo by Jean Tresfon, of the Berg River Dam near Franschoek (33.90S, 19.06E) in early 2018, showing desiccation on the perimeter.

Hydrol. Earth Syst. Sci. Discuss., https://doi.org/10.5194/hess-2018-223
Manuscript under review for journal Hydrol. Earth Syst. Sci.
Discussion started: 2 May 2018

Appendix 2

CPT radiosonde significant-level data up to 850 hPa during case study, with inversion, berg winds (upper) and dry layer (lower) highlighted.

6 Jan 2011 0Z

Pres hPa	Z m	Temp	T dew C	Q g/kg	Dir deg	Spd kt
850	1518	25	-1	4.2	155	16
877	1243	27	2	5.07	138	15
925	771	30.2	6.2	6.47	110	14
931	713	30.8	6.8	6.7	114	14
962	420	32.6	6.6	6.39	135	11
968	364	32.2	7.2	6.62	139	11
974	309	30.8	8.8	7.35	143	11
986	200	26.2	12.2	9.13	151	10
997	102	25.2	13.2	9.65	158	9
1000	76	24	15	10.83	160	9
1004	42	22.2	16.2	11.67	220	10

6 Jan 2011 9Z

Pres hPa	Z m	Temp	T dew C	Q g/kg	Dir deg	Spd kt
850	1558	24	-6	2.89	205	12
909	968	29.4	-14.6	1.36	201	10
925	813	30.4	-13.6	1.45	200	9
938	689	31.4	-10.6	1.83	207	8
944	632	31	-1	3.78	210	8
950	576	29	6	6.21	214	8
962	465	26.6	11.6	8.99	220	7
991	202	28	13	9.58	235	5
1000	122	28.6	12.6	9.24	240	5
1003	95	29.2	12.2	8.97	257	6
1009	42	32.2	7.2	6.35	290	7